J. Electrochem. Sci. Eng. **12(1)** (2022) 59-70; http://dx.doi.org/10.5599/jese.1112

Open Access : : ISSN 1847-9286

https://pub.iapchem.org/ojs/index.php/JESE

Original scientific paper

Development of ciprofloxacin sensor using iron-doped graphitic carbon nitride as transducer matrix: Analysis of ciprofloxacin in blood samples

Hattna Shivarudraiah Vedhavathi[1]; Ballur Prasanna Sanjay[1]; Mahesh Basavaraju[2]; Beejaganahalli Sangameshwara Madhukar[1] and Ningappa Kumara Swamy[1,✉]

[1]*Department of Chemistry, JSS Science and Technology University, Mysuru- 570006, Karnataka, India*
[2]*Department of Chemistry, JSS Academy of Technical Education, Bengaluru- 560060, Karnataka, India*

Corresponding author: ✉kumaryagati@gmail.com; Phone: +91-9741027970, Fax: 0821-2548290

Received: September 15, 2021; Accepted: November 6, 2021; Published: November 17, 2021

Abstract

In the present work, we have synthesized an iron-decorated graphitic carbon nitride (Fe@g-C_3N_4) composite and employed it for electrochemical sensing of ciprofloxacin (CFX). The physicochemical characteristics of the Fe@g-C_3N_4 composite were analyzed with X-ray diffraction (XRD), scanning electron microscopy (SEM), and energy-dispersive X-ray diffraction (EDX) spectroscopy methods. Further, the pencil graphite electrode (PGE) was modified with Fe@g-C_3N_4 composite to get PGE/Fe@g-C_3N_4 electrode and characterized the resultant electrode by cyclic voltammetry (CV) and electrochemical impedance spectroscopy (EIS). Differential pulse voltammetry (DPV) was employed to determine the effect of concentration and interferents. The modified PGE/Fe@g-C_3N_4 electrode demonstrated the exceptional electrochemical performance for CFX identification and quantification with a LOD of 5.4 nM, a wide linear range of 0.001-1.0 µM, and high sensitivity of 0.0018 µA mM^{-1} cm^{-2}. Besides, Fe@g-C_3N_4 modified PGE showed remarkable recovery results in qualitative analysis of CFX in human blood specimens. This research advocates that the Fe@g-C_3N_4 composite acts as an excellent transducer material in the electrochemical sensing of CFX in blood and standard samples. Further, the proposed strategy deduces that the PGE/Fe@g-C_3N_4 sensor can be a prospective candidate for the dynamic determination of CFX in blood serum and possibly ratified as an exceptional drug sensor for therapeutic purposes.

Keywords

quinolone, drug sensor, electrochemical sensor, electrode matrix, differential pulse voltammetry

Introduction

The quinolones are a class of broad spectrum of drugs due to their excellent activity against gram-negative pathogens. They are the choice for patients with intra-abdominal infections together with

anti-anaerobic agents [1-3]. Ciprofloxacin (CFX) continues to be the most efficient quinolone in veterinary and human medication [4]. An immoderate dosage of CFX residues can purport significant antagonistic effects besides causing the ailments such as skin and respiratory infections, chronic bacterial prostatitis, and nosocomial pneumonia [5]. The European Union has set the maximum residue level of ciprofloxacin in milk [6] to be 100 ng mL^{-1}. The presence of CFX and other antimicrobials in the environment is a ground for attention, owing to the possible genesis of resistance to antibiotics. Therefore, developing alternate sensitive and precise sensors to examine the antibiotics in the biological samples (blood) is a dynamic field of the probe [7].

To ascertain the CFX analytical models, like high-performance liquid chromatography, spectrophotometry, capillary electrophoresis, liquid chromatography-mass spectroscopy, spectrofluorimetry, immunoassays, chemiluminescence, impedance spectroscopy, and voltammetry, are performed. Although these methods are sensitive, they are usually elaborate and time-consuming. Moreover, continued specimen pretreatment is essential for the test. Electrochemical methods (impedance spectroscopy, voltammetry) are methods of choice due to their low energy requirement, affordable costs, extraordinary sensitivity, expeditious, and user-friendliness [8-11]. Many biomolecules, including active ingredients in pharmacological formulations and human body fluids, were analysed by electrochemical methodology [12–18]. Diverse designs, procedures, and materials are engaged to promote the sensitivity and selectivity of an electrochemical sensor [15,16]. In the improving electrochemical sensor, nanomaterials were frequently used as transducer elements [19-27]. Previously, carbon-based nanomaterials such as graphene, graphene oxide (GO), multi-walled carbon nanotubes (MWCNTs), reduced graphene oxide (rGO), graphene nanoribbons (GNRs), single-walled carbon nanotubes (SWCNTs), and carbon nanofibers began multiple favourable traits to drive direct electron transfer within the transducer and the electrode surface [28]. Among them, g-C_3N_4 is one of the most promising materials attributable to its unusual two-dimensional graphene-like structure, non-toxicity, extraordinary chemical endurance, easy accesssibility, and photo-responsivity in the visible-light region [29]. Concurrently, metallic nanoparticles (MNPs) in conjunction with carbonaceous substances in various domains like sensors, batteries, drug delivery, medical, solar cells, etc. MNPs possess unique attributes like charge surface-to-volume ratio, superior conductivity, and the capacity to function as an electron-conducting tunnel to magnify the direct electron transfer in an electrochemical sensor [30,31].

Iron (Fe) nanoparticles are acknowledged for their excellent electrocatalytic activity, low cost, non-toxicity, high stability, and fair conductivity, indicating that combining Fe with g-C_3N_4 might improve the sensitivity of the intended sensor [31]. The combination of iron and g-C_3N_4 can potentially magnify the electrochemical sensing characteristics of the electrode surface. The decoration of Fe on the g-C_3N_4 surface can demonstrate a stable sensing platform with good electron transfer characteristics, which ideally suit the construction of novel electrochemical sensing systems. An electrochemical sensor was described with this motivation by modifying a pencil graphite electrode (PGE) with Fe@g-C_3N_4 nanomaterials.

This work demonstrates a new promising electroactive drug sensor for the qualitative and quantitative detection of CFX using g-C_3N_4 and Fe@g-C_3N_4. The proposed sensor manifested an extensive linear detection range, high sensitivity, low detection limit, and selectivity concerning the detection of CFX. Moreover, the sensor considers high accuracy, extensive shelf-life, and reproducibility, indicating that the Fe@g-C_3N_4 is a proper matrix for the sensor fabrication. The real-time application of the advanced sensor is further validated with the analysis of CFX in human blood specimens. Finally, a comprehensive comparison with earlier sensors highlighted the performance

of PGE/Fe@g-C_3N_4. Therefore, it is anticipated that the drug sensor can be a useful tool for biomedical and diagnostic applications.

Experimental

Reagents and equipment

Analytical grade CFX was procured from Sigma-Aldrich (99 %), whereas urea (98 %), Ferric (II) chloride (98 %), acetone (99 %), ascorbic acid (AA) (99 %), uric acid (UA) (99 %) and glucose (99 %) were acquired from Fischer scientific and used as such without further purification. The morphology and elemental composition of the developed sensor were described by scanning electron microscopy (SEM), and energy dispersive X-ray analysis (EDX), and the suggested g-C_3N_4 and Fe@ g-C_3N_4 samples were characterized by a powder X-ray diffractometer (PROTO - AXRD) to authenticate the physical traits like structure, crystallinity, lattice planes, etc. All the voltammetric readings (CV, EIS, and DPV) are conducted utilizing a Biologic Science potentiostat (model SP-150) with the three-electrode configuration.

Synthesis of Fe@g-C_3N_4

The synthesis of g-C_3N_4 was carried out by urea pyrolysis (20 g) using a lid crucible (Isotemp Programmable Muffle Furnace 650-750 Series, Fisher Scientific) in a muffle furnace at 550 °C for 3 h [31]. Finally, the doping of Fe on g-C_3N_4 nanosheets was made by mixing calculated quantities of ferric(II) chloride and 0.6 g of g-C_3N_4 nanosheets in 50 mL of acetone with constant stirring. The resulting suspension was agitated for two hours at ambient temperature, centrifuged for 15 min at around 6000 rpm, and rinsed many times with acetone to eliminate aggregates. The color of the withered specimens slightly shifted from pale yellow to imperceptibly reddish-brown upon the doping of iron [29].

Fabrication of CFX sensor with Fe@g-C_3N_4

A cylindrically shaped pencil graphite rod with a diameter of 3 mm (surface area: 0.07068 cm^2) was utilized as a working electrode. Further, the electrode was modified by taking a tiny portion of the rod and polished along one face. A copper wire was fastened to secure the electrical contact flanked by the electrode and the potentiostat. To obtain a shiny surface, PGE was polished using emery paper (80 and 300 Grit) and consequently, with the electrode polishing solution containing alumina and silica using electrode polishing tool kit (PK-3 brand kit). Then, the polished PGE was sonicated and eventually washed with milli-Q water and dried at room temperature to eliminate loosely bounded shreds. The prepared bare PGE was further deposited with 3 µl of 5 mg mL^{-1} stock solution of Fe@ g-C_3N_4 by drop-casting method and eventually, the electrode was dried at ambient temperature to get the working electrode PGE/Fe@g-C_3N_4.

Electrochemical studies

The electrochemical investigations were performed in a three-electrode cell, where PGE was used as a working electrode (surface area: 0.07068 cm^2), saturated calomel electrode as the reference electrode, and platinum wire as the counter electrode. All electrochemical characteristics of bare and modified PGEs were performed in phosphate buffer solution (PBS) of pH 7.0. The charge transfer at the electrode/electrolyte interface of the altered electrode was studied in the frequency range of 100 kHz to 0.1 Hz using the EIS technique, with 5 mM $[Fe(CN)_6]^{3-/4-}$ as the electrochemical probe. The probe of EIS had operated in 0.1M PBS (pH 7.0) constituting 1 mM $[Fe(CN)_6]^{4-/3-}$, and at an amplitude of 5 mV and frequencies within 100 kHz and 0.1Hz range.

Preparation of sample for real analysis

The serum samples collected from normal individuals (taking their inscribed consent) were refrigerated till examination. 5 mL of serum was treated with an equivalent volume of methanol as a serum desaturating and precipitating agent. The conduits were vortexed for 10 min and then centrifuged for 40 min at 5000 rpm to eliminate the protein residues. The supernatants were diluted up to 10 mL with the 0.1 M PBS buffer solution of pH 7.0. The standard addition method was employed for calculating the recoveries of the spiked CFX in human serum. The percentage recovery and detection precision were computed based on the known amount of spiked CFX (*R*) and empirical values (*E*) using equations 1 and 2.

$$\text{Accuaracy}, \% = \frac{R-E}{R}100 \quad (1)$$

$$\text{Recovery}, \% = \frac{R}{E}100 \quad (2)$$

Results and discussion

X-ray diffraction and FT-IR studies

Figure 1A shows XRD patterns of the nanosheets of the integrated g-C_3N_4 and Fe@g-C_3N_4. A strong diffraction peak at 27.3° demonstrates strong interlayer interactions of aromatic rings, indexed as the (002) planes for g-C_3N_4. The smaller diffraction signal at around 13.1°, listed as (100), is associated with the in-plane structural perpetual motif, *i.e.,* the continuous tri-s-triazine structures [32]. Besides, the depth of the (002) peak had substantially diminished and expanded for g-C_3N_4 nanosheets [33]. The resulting doping with Fe evidenced no change of the crystal phase of g-C_3N_4. The location of diffraction peaks for nanosheets Fe@g-C_3N_4 switched to a steadily higher angle for nanosheets of g-C_3N_4. The peak intensity diminished, and the diffraction peak width broadened for iron content, implying the presence of excess Fe species caused the host-guest interactions and polymeric condensation inhibition. It is further evident that the iron is chemically coordinated to g-C_3N_4 via Fe-N bonds [34].

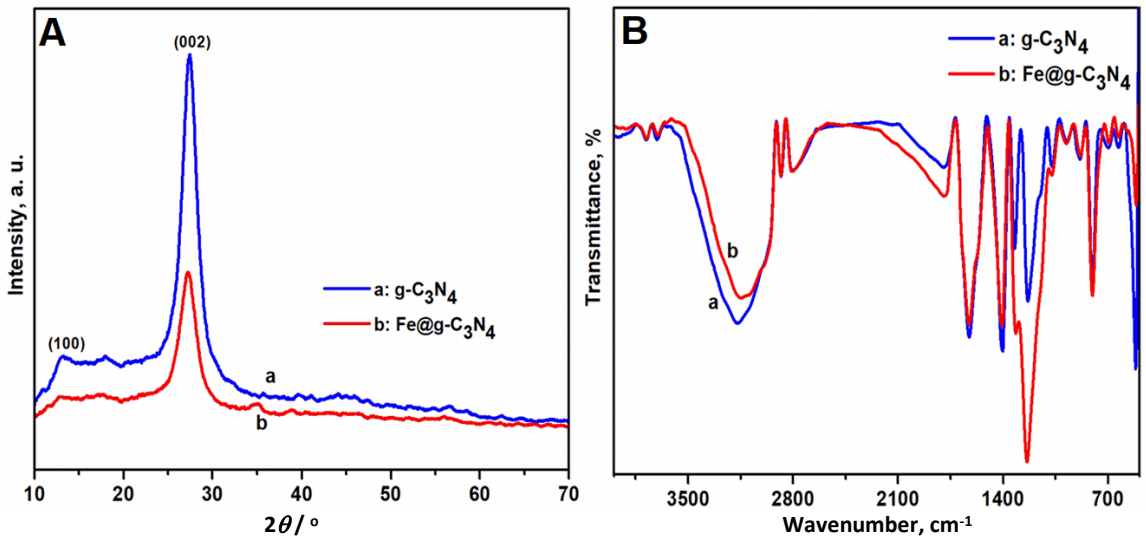

Figure 1. *A - XRD data of g-C_3N_4 and Fe@g-C_3N_4, and B - IR spectrum of g-C_3N_4 and Fe@g-C_3N_4*

Figure 1B shows the FT-IR spectra of the g-C_3N_4 and Fe@g-C_3N_4 nanosheets. From Figure 1B, the extended absorption band at nearly 3155 cm^{-1}, assigned to the stretching vibrational modes of surplus N–H components connected with uncondensed amino groups [35,36], can be identified. The

peak at 1633 cm^{-1} is classified as vibrational stretching mode, whereas aromatic C-N stretching vibrations of heterocyclic rings matched with the bands at 1415, 1400, and 1234 cm^{-1} [26]. The specific particular peak at 807 cm^{-1} confirmed the s-triazine ring system [37]. Further, it is evidenced from Figure 1B that the intensity of the peaks reduced with an increase in Fe content in the Fe@g-C_3N_4, and the principal characteristic bands of g-C_3N_4 nanosheets change to smaller wavenumbers (redshift) intimates that the C-N and C=N bonds are weakened [29]

SEM and EDS analysis

The g-C_3N_4 and Fe@g-C_3N_4 synthesis was demonstrated by SEM and EDS study. Figures 2A and 2B denote the SEM image of integrated g-C_3N_4 and Fe@g-C_3N_4 nanocomposite. The micrographs were obtained at 3,000 magnifications by an expediting voltage of 5.0 kV LED. The sheets-like morphology evidences a greater surface area for the catalytic reactions between target and transducer interface [38].

Figure 2C shows the EDS spectrum of the synthesized material, and it reveals elemental composition. The EDS data illustrated the presence of carbon (C) 51.92 %, nitrogen (N) 31.24 %, oxygen (O) 2.96 %, and iron (Fe) 13.88 % in the Fe@g-C_3N_4 sample, indicating that Fe-doped g-C_3N_4 has a pretty high rate of purity, and it comprises solely four elements. These essential considerations made on EDS interpretation insinuate the purity of the substance.

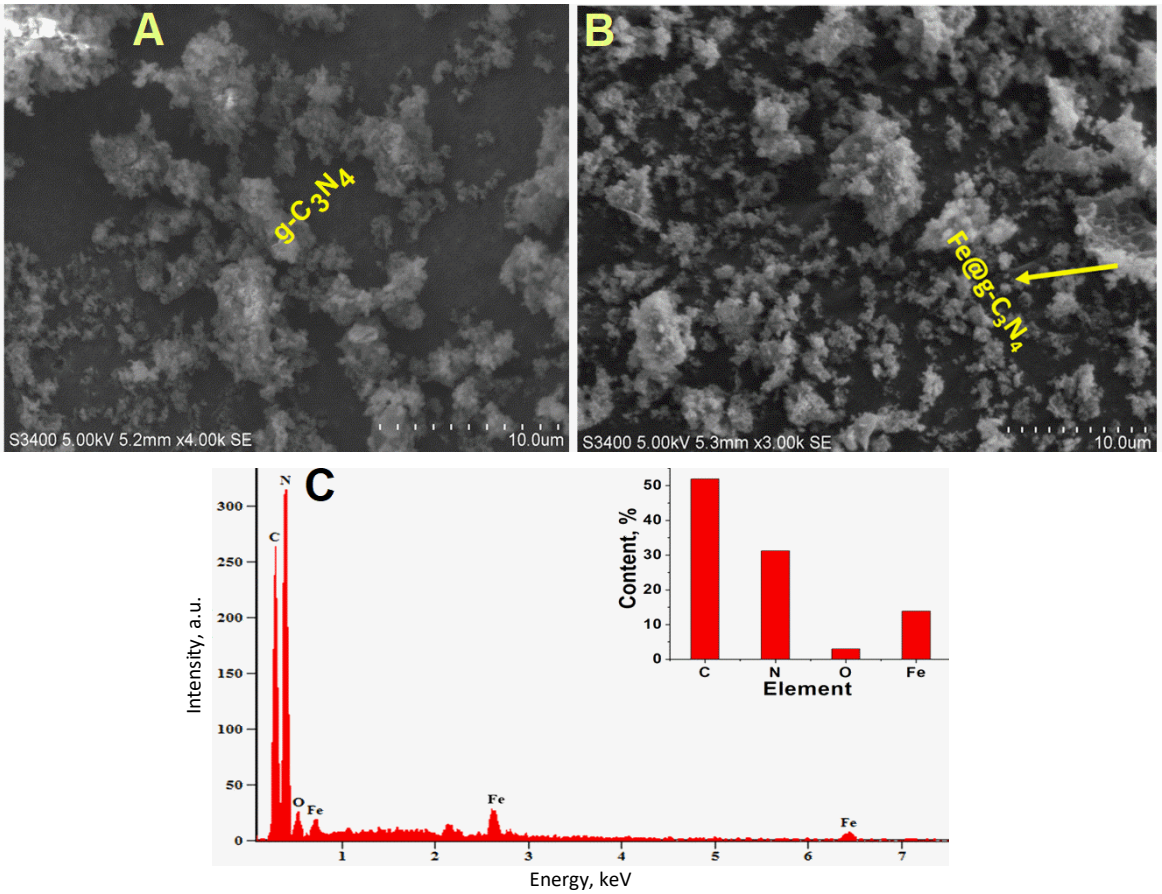

Figure 2. *A - SEM image of g-C_3N_4, B - SEM image of Fe@g-C_3N_4, (C) EDX of Fe@g-C_3N_4, (Inset: elemental composition)*

Electrochemical assessment of the modified PGE

The electrochemical response of the modified PGE was monitored by CV using a 5 mM $[Fe(CN)_6]^{3-/4-}$ as an electrochemical mediator in 0.1 M PBS buffer (pH 7.0). The CV of the bare PGE shows a

well-defined quasi reversible oxidation and reduction peaks with a peak-to-peak separation (ΔEp) of 201.6 mV (Figure 3A, curve a). The peak current increased after the deposition of 3 µl Fe@g-C_3N_4, which resulted in peak separation (ΔEp) of 271.2 mV (Figure 3A, curve b). The increase in current response and stability of the CV curve suggests the successful deposition of Fe@g-C_3N_4 on the PGE electrode surface.

EIS spectra of PGE and PGE/Fe@g-C_3N_4 recorded in 1 mM $[Fe(CN)_6]^{4-/3-}$ PBS solution Figure 3B are displayed in the Nyquist diagram. From the EIS data, the charge transfer resistance (R_{ct}) could be calculated from the best fit of the Randles electrical equivalent circuit. The R_{ct} for bare PGE is 78.73 kΩ, and after the addition of Fe@g-C_3N_4, R_{ct} is reduced to 19.41 kΩ on account of the higher rate of electron transfer between the redox probe and electrode surface. Reduction in R_{ct} values on the deposition of Fe@g-C_3N_4 is clearly in agreement with CV results, and it further confirms the successful electrode deposition.

Randles–Sevcik equation (Equation 3) was used to validate the improved catalytic response of modified PGE in terms of increased active electrode surface area [39].

$$I_p = (2.69\ 10^5)n^{3/2}A_0D_R^{1/2}v^{1/2} \quad (3)$$

where I_p is the anodic peak current of PGE/Fe@g-C_3N_4 (I_p = 1.38×10^{-4} A), and n is the number of electrons transferred in the redox reaction of CFX (n = 2). A / cm^2 is the electroactive surface area to be determined, D_R (cm^2/s) is the solution diffusion coefficient (6×10^{-6} for $[Fe(CN)_6]^{4-}$). C_0 (mol/cm^3) is the concentration of the reaction species in the electrolyte (10^{-6} for $[Fe(CN)_6]^{4-}$), and v (V/s) is the scan rate [40]. From this equation, the PGE/Fe@g-C_3N_4 active electrode surface area was calculated to 3.94 cm^2, ensuring the high electrocatalytic surface area for the modified electrode [41].

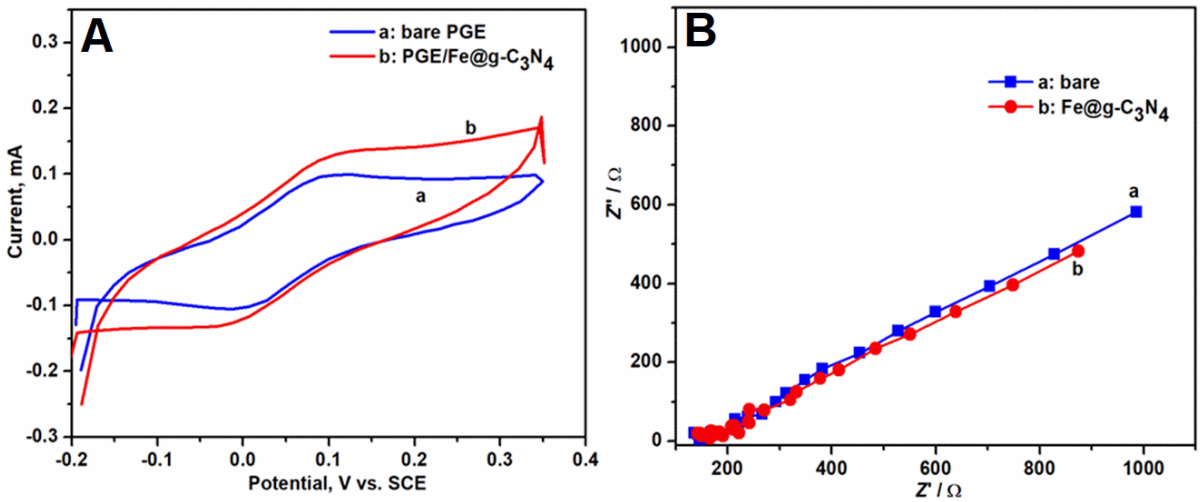

Figure 3. *A - CVs of 5 mM $[Fe(CN)_6]^{3-/4-}$ solution obtained held at (a) bare PGE, (b) PGE/Fe@g-C_3N_4(3 µl); B - Nyquist diagrams of EIS data of (a) bare PGE, (b) PGE/Fe@g-C_3N_4 (3 µl)*

Effect of scan rate and pH

Figure 4A shows the effect of the scan rate on the modified PGE/Fe@g-C_3N_4 for various scan rates like from 25 up to 375 mV s^{-1} in 10 µM solution of CFX. The oxidation peak current increases with the scan rate. Figure 4B shows the linear relationship between the current peak height and the square root of the scan rate with the regression coefficient of R^2=0.9966. It is because the larger surface area facilitates faster electron transfer.

Further, the regression analysis of log I_p versus log v plot gives a relation of log I_p=0.7601 log v + + 1.7926; R^2= 0.9973 with the slope close to 1. The value of slope of log Ip versus log v confirms that the electrode process is dominantly diffusion-controlled [41].

To know the effect of pH on the electrochemical properties of the proposed sensor, the electrochemical performance of the Fe@g-C_3N_4 decorated PGE electrode was investigated in different pHs in the range 3 - 9) in the presence of 10 µM CFX in PBS buffer solution. From Figure 4C, the current response of the sensor at different pH values reveals that the oxidation peak reached the maximum at pH 7.0. Therefore, pH 7.0 was adopted for all further analyses.

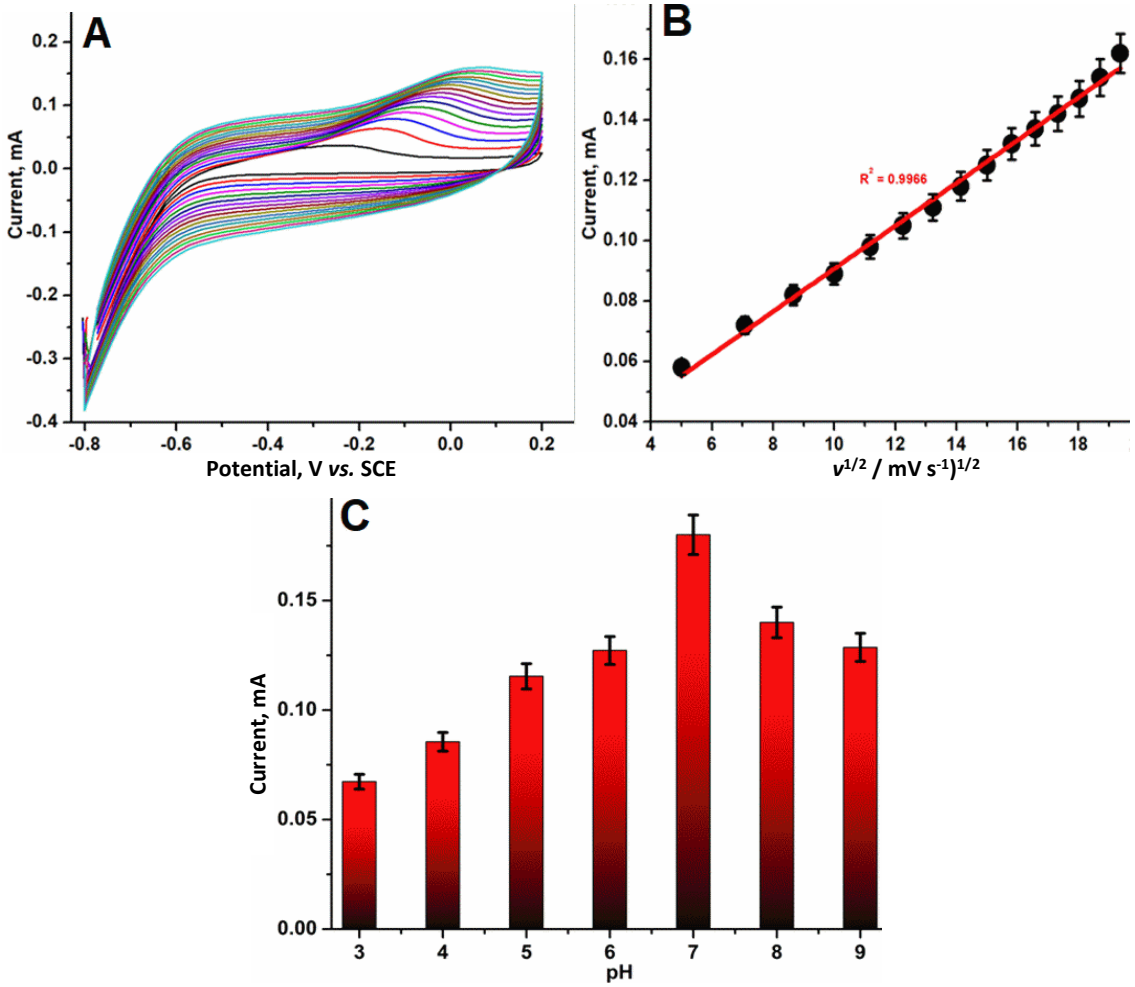

Figure 4. *A - CVs of PGE/Fe@g-C_3N_4 in 0.1 M PBS (pH 7) containing 10 µM CFX at different scan rates; B - Plot of Anodic peak current* vs. $v^{-1/2}$ *(c) Effect of pH on the response of PGE/Fe@gC_3N_4 modified electrode*

Electrochemical determination of CFX

Figure 5A shows cyclic voltammograms of PGE/Fe@g-C_3N_4 in the presence of different concentrations of CFX (1-100 µM) in nitrogen saturated PBS (pH 7.0) at a scan rate of 50 mV s^{-1}. With the increase in the concentration of CFX, the oxidation peak current proportionately increases at the Fe@g-C_3N_4 modified electrode. Oxidation of CFX is the electrochemical reaction occurring at the electrode/electrolyte interface, as shown in Scheme 1. The anodic peak current increased linearly from 1 to 100 µM of CFX with a correlation coefficient (R^2) of 0.9675. Hence, this proves the authenticity of the sensor performance.

The DPV experiment was conducted in 0.1 PBS solution in the potential range -0.1 to 1.5 V at smaller concentrations of CFX. Fig 5B illustrates the DPV current response from 1 to 1000 nM of CFX, and it is clear from Fig 5B that there is a linear relationship between current and CFX concentration with a correlation coefficient of R^2 = 0.9968. The data from DPV experiments were used to compute the analytical quantities of the sensor *i.e.,* the limit of detection (LOD), sensitivity, and quantification limit (LOQ) (equations 4, 5, and 6) [42].

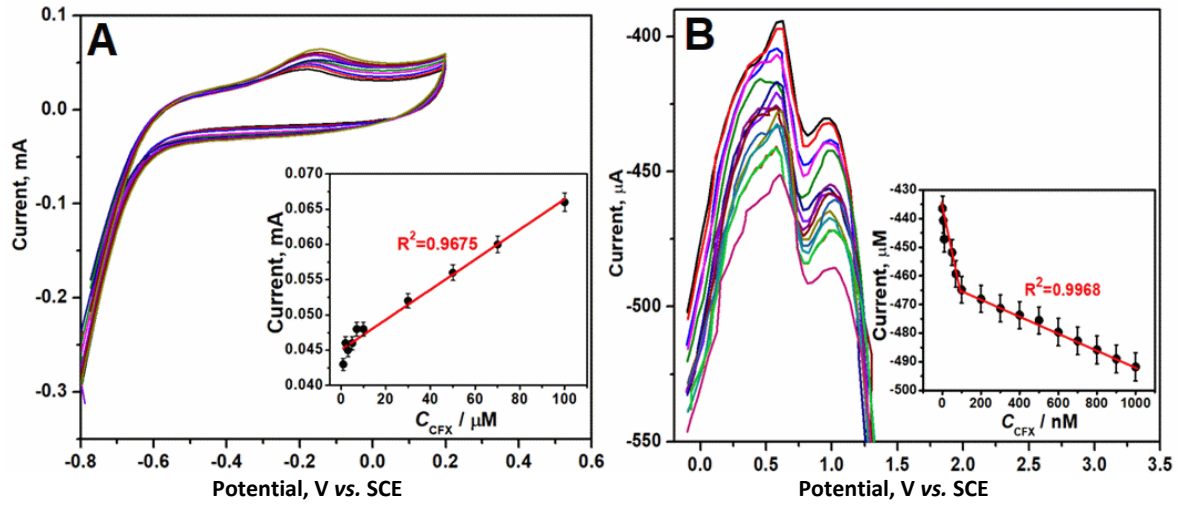

Figure 5. *A - CVs of PGE/Fe@g-C_3N_4 electrode at various CFX concentrations (1 to 100 µM) in 0.1M PBS at pH 7, Inset: calibration plot of current Vs CFX concentration; B - DPVs of the PGE/Fe@g-C_3N_4 electrode in the presence of varying CFX concentrations (1 to 1000 nM) in 0.1 M PBS solution; Inset: peak current Vs CFX concentration*

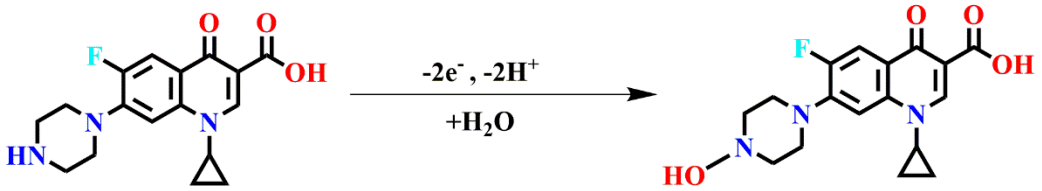

1-cyclopropyl-6-fluoro-4-oxo-7-(piperazin-1-yl)-1,4-dihydroquinoline-3-carboxylic acid

1-cyclopropyl-6-fluoro-7-(4-hydroxypiperazin-1-yl)-4-oxo-1,4-dihydroquinoline-3-carboxylic acid

Scheme 1*. The electrocatalytic interaction at the interface is represented using chemical equations*

$$LOD = 3\sigma / S \quad (4)$$

$$Sensitivity = I / A \quad (5)$$

$$LOQ = 10\sigma / S \quad (6)$$

Here, σ represents the standard deviation of the blank, and S indicates the slope of the calibration plot (Inset: Figure 5B). The sensitivity, LOQ, linear range, and LOD determined using the above experimental data are 0.0596 µA $mM^{-1}cm^{-2}$, 0.0018 µM, 0.001 to 1.0 µM, and 5.4 nM, respectively. The overall analytical performance of the suggested Fe@g-C_3N_4 based sensor is in accordance with those already reported in the literature (Table 1) [43-47]. The superior performance characteristics exhibited by the PGE/Fe@g-C_3N_4 sensor are explicitly related to the composite matrix's synergic effects [48]. This suggests that the as-developed sensor can be a promising tool in the analysis of CFX.

Table 1. Comparison of different electrochemical sensors for the determination of CFX

Matrix	Linear range of detection of CFX, µM	LOD, nM	References
$MgFe_2O_4$-MWCNT/GCE	0.1 - 1000	10	[43]
MWCNT-GCE	40 - 1000	6000	[44]
TiO_2/PB/AuNPs/CMK3/Nafion/GE	1 - 10	108	[45]
β–CD/MWCNT/GC	10 - 80	5	[46]
Boron doped diamond electrode	0.15 - 2.11	50	[47]
PGE/Fe@g-C_3N_4	0.001-1.0	5.4	Proposed work

Effects of interferents

The proposed sensor was subjected to radical scavenging experiments to affirm its selectivity. The DPV responses were recorded after the additions of 50 µM of some common interferents like AA, UA,

glucose, Ca^{2+}, and Mg^{2+} to 10 µM CFX in 0.1 PBS buffer solution. The obtained DPV responses are exhibited in Figure 6. Figure 6 discloses no significant variation in the current peaks despite the residence of interferents, implying the selectivity and robustness of the sensor for field purposes.

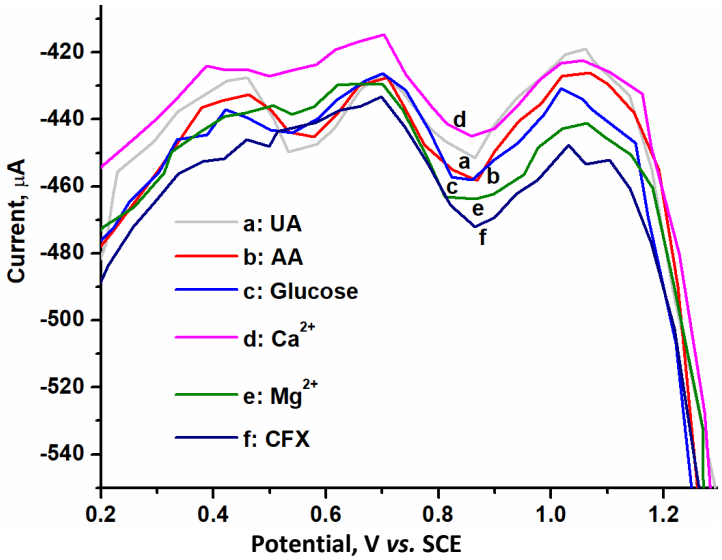

Figure 6. *DPVs of PGE/Fe@g-C_3N_4 electrode in the presence of 10 µM CFX and 50 µM additions of interferents such as uric acid, ascorbic acid, glucose, Ca^{2+}, and Mg^{2+} in PBS buffer (pH 7.0)*

Repeatability, reproducibility, and stability

These experiments are crucial to argue on the sensor's practical applicability and reliability. The repeatability of the sensor performance was tested by measuring the CV response for 10 µM CFX in 0.1M PBS solution for twenty electro-analytical cycles between −0.1 to 1.5 V at a scan rate of 50 mV s^{-1}. Further, we examined the reproducibility of the PGE/Fe@g-C_3N_4 electrodes by preparing a set of five distinct electrodes using a method described in the experimental section. The current response of these electrodes was measured by CV in 0.1 M PBS comprising 10 µM CFX. The estimated magnitude of the current response under identical circumstances depicts comparable electro-chemical properties for the sensor with a suitable shift in peak current, demonstrating an agreeable reproducibility as apparent from Fig 7A.

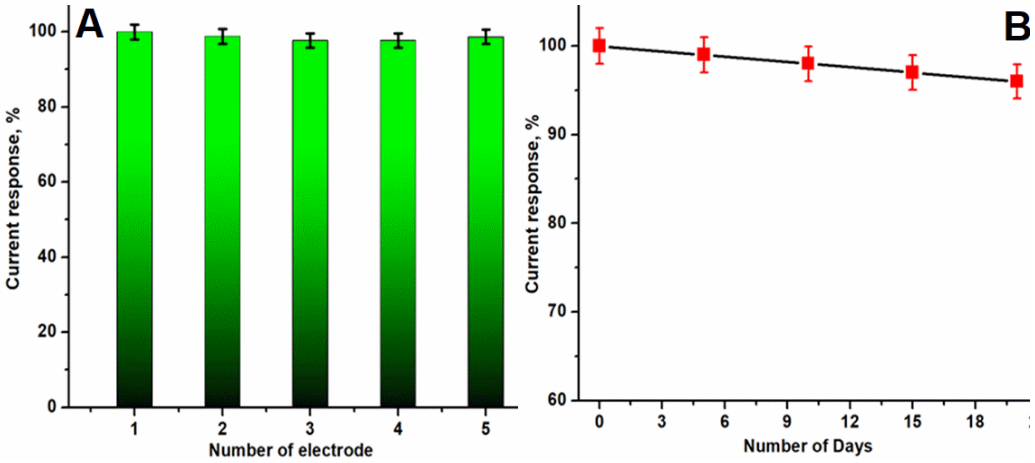

Figure 7. *A - The peak current measured for 10 µM CFX in 0.1M PBS (pH) with five separately tailored PGE/Fe@g-C_3N_4 to symbolize the sensor's repeatability; B - Stability of the sensor in the presence of 10 µM CFX*

The storage stability of the PGE/Fe@g-C_3N_4 electrode had been determined steadily for up to twenty days, and the results are shown in Figure 7B. The current response for 10 µM CFX was

monitored at regular intervals, and the developed sensor retained 100, 98.01, 97.13, 97.02, and 96 % of the initial current response after 0, 5, 10, 15, and 20 days of storage, respectively, suggesting that the developed sensor exhibits a high level of stability in the detection of CFX.

Real sample analysis

The potency of the proposed sensor in practical applications was ascertained by analyzing CFX in human blood specimens. The actual samples were diluted with PBS in equal proportions, accompanied by spiking a known quantity of CFX to them. The responses were measured, and the observed percentage of the recovery is registered in Table 2. As noted, the results attained are good, with insignificant errors and hence the developed sensor might be used for the determination of CFX in biological fluids. It ratifies the generated sensor for primary specimen analysis. The worthy administration characteristics buttressed by the PGE/Fe@g-C_3N_4 sensor are completely ascribed to the synergic effect of the composite matrix.

Table 2. *Detection of CFX using proposed Fe@g-C_3N_4 sensor in blood samples*

Sample	Amount of CFX spiked, nM	Amount of CFX found, nM	Recovery, %	Accuracy, %
A	100	98.9	100.5	100.1
B	100	100.6	99.7	99.8

Conclusion

In the present work, we developed an electrochemical sensor using Fe@g-C_3N_4 composite as a working electrode matrix. The physical, chemical and electrochemical investigations of the Fe@g-C_3N_4 matrix confirmed the sensor's stability, conductivity, and electrocatalytic nature. It has the advantage of a low detection limit (5.4 nM) and a wide linear range (0.001-1.0 µM) in the detection of CFX. The offered sensor manifested an exceptional selectivity, sensitivity (0.0596 µA mM^{-1} cm^{-2}) and reproducibility regarding the CFX determination. This sensor proved comparatively improved performance than various CFX sensors reported earlier in the literature. Remarkably, the success had interlaced by the cost-effective matrix and optimized material usage of the sensor. The parameters including storage stability, reproducibility, and repeatability were studied. The PGE/Fe@g-C_3N_4 sensor may be an alternative to the reported sensors for detecting and quantifying CFX in blood, environmental and industrial specimens.

Acknowledgments: *The authors successfully acknowledge the colossal support from the Department of Chemistry, JSS Science and Technology University, Mysuru-570006, India and Department of Chemistry and Principal, JSSATE Bengaluru, Karnataka, India*

References

[1] J. S. Solomkin, H. H. Reinhart, E. P. Dellinger, J. M. Bohnen, O. D. Rotstein, S. B. Vogel, H. H. Simms, C. S. Hill, H. S. Bjornson, D. C. Haverstock, H. O. Coulter, R. M. Echols, *Annals of Surgery* **223** (1996) 303-315. https://doi.org/10.1097/00000658-199603000-00012

[2] A. R. Abadia, J. J. Aramayona, M. J. Muńoz, J. M. P. Delfina, M. A. Bregante, *Journal of Veterinary Medicine* **42** (1995) 505-511. https://doi.org/10.1111/j.1439-0442.1995.tb00405.x

[3] R. Davis, A. Markham, J. A. Balfour, *Drugs* **51** (1996) 1019-1074. https://doi.org/10.2165/00003495-199651060-00010

[4] H. H. H. Mohammed, G. E.-D. A. A. Abuo-Rahma, S. H. Abbas, E. S. M. N. Abdelhafez, *Current Medicinal Chemistry* **26** (2018) 3132-3149. https://doi.org/10.2174/0929867325666180214122944

[5] B. Huang, Y. Yin, L. Lu, H. Ding, L. Wang, T. Yu, J. J. Zhu, X. D. Zheng, Y. Z. Zhang, *Journal of Zheijang University Science B* **11** (2010) 812-818. https://doi.org/10.1007/s10967-010-0571-z
[6] M. Tumini, O. Nagel, M. P. Molina, R. Althaus, *International Dairy Journal* **64** (2017) 9–13. https://doi.org/10.1016/j.idairyj.2016.08.008
[7] J. B. Xiao, C. S. Yang, F. L. Ren, X. Y. Jiang, M. Xu, *Measurement Science and Technology* **18** (2007) 859-866. https://doi.org/10.1088/0957-0233/18/3/039
[8] H. Karimi-Maleh, F. Karimi, L. Fu, A. L. Sanati, M. Alizadeh, C. Karaman, Y. Orooji, *Journal of Hazardous Materials* **423** (2022) 127058. https://doi.org/10.1016/j.jhazmat.2021.127058
[9] H. Karimi-Maleh, Y. Orooji, F. Karimi, M. Alizadeh, M. Baghayeri, J. Rouhi, S. Tajik, H. Beitollahi, S Agarwal, V. K. Gupta S. Rajendran, *Biosensors and Bioelectronics* **184** (2021) 113252. https://doi.org/10.1016/j.bios.2021.113252
[10] H. Karimi-Maleh, M. L. Yola, N. Atar, Y. Orooji, F. Karimi, P. S. Kumar, J. Rouhi, M. Baghayeri, *Journal of Colloid and Interface Science* **592** (2021) 174-185. https://doi.org/10.1016/j.jcis.2021.02.066
[11] C. Karaman, O. Karaman, B. B. Yola, I. Ulker, N. Atar, M. L. Yola, *New Journal of Chemistry* **45** (2021) 11222-11233. https://doi.org/10.1039/D1NJ02293H
[12] C. Karaman, O. Karaman, N. Atar, M. L. Yola, *Microchimica Acta* **188** (2021) 182. https://doi.org/10.1007/s00604-021-04838-6
[13] R. N. Goyal, V. K. Gupta, S. Chatterjee, *Electrochimica Acta* **53** (2008) 5354-5360. https://doi.org/10.1016/j.electacta.2008.02.059
[14] R. N. Goyal, V. K. Gupta, N. Bachheti, *Analytica Chimica Acta* **597** (2007) 82-89. https://doi.org/10.1016/j.aca.2007.06.017
[15] H. Bagheri, A. Shirzadmehr, M. Rezaei, *Journal of Molecular Liquids* **212** (2015) 96-102. https://doi.org/10.1016/j.molliq.2015.09.005
[16] H. Bagheri, A. Afkhami, Y. Panahi, H. Khoshsafar, A. Shirzadmehr, *Materials Science and Engineering C* **37** (2014) 264-270. https://doi.org/10.1016/j.msec.2014.01.023
[17] N. Ozcan, C. Karaman, N. Atar, O. Karaman, M. L. Yola, *Journal of Solid State Science and Technology* **9(12)** (2020) 121010. https://doi.org/10.1149/2162-8777/abd149
[18] C. P. Boke, O. Karaman, H. Medetalibeyoglu, C. Karaman, N. Atar, M. L. Yola, *Microchemical Journal* **157** (2020) 105012. https://doi.org/10.1016/j.microc.2020.105012
[19] M. Baghayeri, H. Veisi, H. Veisi, B. Maleki, H. Karimi-Maleh, H. Beitollahi, *RSC Advances* **4(91)** (2014) 49595-49604. https://doi.org/10.1039/C4RA08536A
[20] M. A. Khalilzadeh, H. Karimi-Maleh, A. Amiri, F. Gholami, *Chinese Chemical Letters* **21(12)** (2010) 1467-1470. https://doi.org/10.1016/j.cclet.2010.06.020
[21] A. A. Ensafi, E. Khoddami, B. Rezaei, H. Karimi-maleh, *Colloids and Surfaces B* **81(1)** (2010) 42-49. https://oi.org/10.1016/j.colsurfb.2010.06.020
[22] H. Medetalibeyoğlu, M. Beytur, S. Manap, C. Karaman, F. Kardaş, O. Akyıldırım, M. L. Yola, *ECS Journal of Solid State Science and Technology* **9(10)** (2020) 101006. https://doi.org/10.1149/2162-8777/abbe6a
[23] C. Somaye, A. Mohammad H. Taher, H. Karimi-Maleh, K. Fatmeh, S. N. Mehdi, A. Marzieh, A.O. Amani, E. Nevin, K. Praveen, R. Yegya, K. Ceren, *Chemosphere* **287(2)** (2022) 132187. https://doi.org/10.1016/j.chemosphere.2021. 132187
[24] A. A. ENSAFI, D. T. Samira, K. M. Hassan, *Analytical Sciences* **27(4)** (2011) 409. https://doi.org/10.2116/analsci.7.409
[25] J. A. Cruz-Navarro, F. Hernandez-Garcia, G. A. Alvarez Romero, *Coordination Chemistry Reviews*, **412** (2020) 213263. https://doi.org/10.1016/j.ccr.2020.213263.
[26] J. A. Cruz-Navarro, F. Hernández-García, L. H. Mendoza-Huizar, V. Salazar-Pereda, J. Á. Cobos-Murcia, R. Colorado-Peralta, G. A. Álvarez-Romero, *Solids* **2** (2021) 212-231. https://doi.org/10.3390/solids2020014

[27] S. Sandeep, A. S. Santhosh, N. K. Swamy, G. S. Suresh, J. S. Melo, N. A. Chamaraja, *New Journal of Chemistry* **42** (2018) 16620–16629. https://doi.org/10.1039/C8NJ02325E
[28] H. Ishiguro, Y. Yao, R. Nakano, M. Hara, K. Sunada, K. Hashimoto, J. Kajioka, A. Fujishima, Y. Kubota, *Applied Catalysis B* **129** (2013) 56-61. https://doi.org/10.1016/j.apcatb.2012.09.012
[29] K. Sunada, T. Watanabe, K. Hashimoto, *Environmental Science & Technology* **37** (2003) 4785-4789. https://doi.org/10.1021/es034106g
[30] J. Liu, T. Zhang, Z. Wang, G. Dawson, W. Chen, *Journal of Materials Chemistry* **21** (2011) 14398. https://doi.org/10.1039/C1JM12620B
[31] F. Goettmann, A. Fischer, M. Antonietti, A. Thomas, *Angewandte Chemie* **45** (2006) 4467-4471. https://doi.org/10.1002/anie.200600412
[32] X. Zhang, X. Xie, H. Wang, J. Zhang, B. Pan, Y. Xie, *Journal of the American Chemical Society* **135** (2013) 18–21. https://doi.org/10.1021/ja308249k
[33] X. Wang, X. Chen, A. Thomas, X. Fu, M. Antonietti, *Advanced Materials* **21** (2009) 1609-1612. https://doi.org/10.1002/adma.200802627
[34] G. Zhang, J. Zhang, M. Zhang, X. Wang, *Journal of Materials Chemistry* **22** (2012) 8083. https://doi.org/10.1039/C2JM00097K
[35] S. C. Yan, Z. S. Li, Z. G. Zou, *Langmuir* **25** (2009) 10397-10401. https://doi.org/10.1021/la900923z
[36] K. S. Siddegowda, B. Mahesh, N. A. Chamaraja, B. Roopashree, N. Kumara Swamy, G. S. Nanjundswamy, *Electroanalysis* **32** (2020) 2183–2192. https://doi.org/10.1002/elan.202000010
[37] Y. Li, J. Zhang, Q. Wang, Y. Jin, D. Huang, Q. Cui, G. Zou, *Journal of Physical Chemistry B* **114** (2010) 9429-9434. https://doi.org/10.1021/jp103729c
[38] S. Sarkar, N. Kamboj, M. Das, T. Purkait, A. Biswas, R. S. Dey, *Inorganic Chemistry* **59** (2020) 1332-1339. https://doi.org/10.1021/acs.inorgchem.9b03042
[39] B. P. Sanjay, N. Kumara Swamy, S. R. Yashas, S. Sandeep, *Journal of the Electrochemical Society* **168** (2021) 076511. https://doi.org/10.1149/1945-7111/ac1495P
[40] P. Zhu Y. Zhao, *Materials Chemistry and Physics* **233** (2019) 60-67. https://doi.org/10.1016/j.matchemphys.2019.05.034
[41] N. P. Shetti, S. J. Malode, S. T. Nandibewoor, *Analytical Methods* **7** (2015) 8673-8682. https://doi.org/10.1039/C5AY01619C
[42] B. P. Sanjay, S. Sandeep, A. S. Santhosh, C. S. Karthik, D. N. Varun, N. Kumara Swamy, P. Mallu, K. S. Nithin, J. R. Rajabathar, K. Muthusamy, *Chemosphere* **287** (2022) 132153. https://doi.org/10.1016/j.chemosphere.2021.132153
[43] S. R. Yashas, S. Sandeep, B. P. Shivakumar, N. K. Swamy, *Analytical Methods* **11** (2019) 4511-4519. https://doi.org/10.1039/C9AY01468C
[44] A. A. Ensafi, A. R. Allafchian, R. Mohammadzadeh, *Analytical Sciences* **28** (2012) 705-710 (2012). https://doi.org/10.2116/analsci.28.705
[45] L. Fotouhi, M. Alahyari, *Colloids Surfaces B Biointerfaces* **81** (2010) 110-114. https://doi.org/10.1016/j.colsurfb.2010.06.030
[46] A. Pollap, K. Baran, N. Kuszewska, J. Kochana, *Journal of Electroanalytical Chemistry* **878** (2020) 114574. https://doi.org/10.1016/j.jelechem.2020.114574
[47] J. M. Garrido, M. Melle-Franco, K. Strutynski, F. Borges, C. M. Brett, E. M. P. Garrido, *Journal of Environmental Science and Health* **52** (2017) 313-319. https://doi.org/10.1080/10934529.2016.1258864
[48] K. S. Siddegowda, B. Mahesh, N. Kumara Swamy, *Sensors and Actuators A* **280** (2018) 277-286. https://doi.org/10.1016/j.sna.2018.07.049